Journal of Material Cycles and Waste Management (2024) 26:331–345
https://doi.org/10.1007/s10163-023-01838-x

ORIGINAL ARTICLE

Sustainable composite cement prepared by two different types of iron slag

Mohamed Heikal[1] · Mohamed A. Ali[2] · Sahar M. Ibrahim[1] · Hazem I. Bendary[3]

Received: 19 February 2023 / Accepted: 8 October 2023 / Published online: 6 November 2023

Abstract

The utilization of two kinds of iron slag in the production of pozzolanic cement is introduced. A series was created with a fixed percentage of OPC (30%) and varying amounts of imported granulated blast-furnace slag (IGBFS) and air-cooled slag (ACS) at which imported IGBFS was substituted by ACS with the mass ratios of 10, 20, and 30%. Physico-mechanical properties and hydration parameters of the hardened pastes were examined at different time intervals. Furthermore, the aggressive attack of seawater on chosen specimens was studied for up to one year of immersion. The hardened composite cement pastes were tested in terms of weight loss, compressive strength, bulk density, total porosity, and free lime at different thermally treated temperatures starting at 105 °C and ending at 800 °C for 2 h of a socking period to investigate its thermal characteristics. XRD, IR, and DTA/TGA techniques were used to examine some chosen samples. The results revealed that the incorporation of ACS reduces the water consistency and prolongs setting times. Compressive strengths are higher in samples containing 10% ACS than those specimens containing 20–30 wt% and without ACS. A 7% reduction in the compressive strength was achieved by A1 (30%OPC and 70% IGBFS), which is the lowest one over 1 year of exposure to seawater. The incorporation of ACS at the expense of IGBFS tends to lower the strength but tends to enhance the bulk density.

Keywords Physico-mechanical properties · Composite cement · Hydration products · Thermally treated temperatures · Exposure to seawater attack

Introduction

Urbanization growth necessitates infrastructure expansion, which raises the output of ordinary Portland cement, the most often used binder. Approximately 8% of the world's anthropogenic CO_2 emissions are caused by the manufacturing of Portland cement [1]. Recently CO_2 emissions have been reduced primarily by three methods (e.g., energy efficiency improvement, fuel switching using waste as an alternative fuel, and blended cement using industrial by-products) [2–4]. Iron slag is perhaps one of the earliest additions that were made to cement to improve its strength and chemical durability [5]. Blast-furnace slag (BFS) is a by-product of the iron-making process that is produced when the aluminosilicate waste from the iron ores is fused with limestone and coke ash. This procedure results in the formation of a molten slag which floats on the surface of the iron. After that, it is cooled and withdrawn. Based on the cooling process, there is three different forms of iron slag are formed, namely granulated, air-cooled and pelletized blast-furnace slags which are reused in many applications, especially concrete works [6–8]. The rapid cooling of iron slag with water is responsible for its amorphous nature which exceeds 95% amorphous calcium aluminosilicate. This kind of slag is known as granulated blast furnace slag (IGBFS) [9–12]. Incorporating IGBFS in concrete improves various properties, including early hydration, strength, permeability, and sulfate resistance, while a higher proportion of IGBFS reduces rebar corrosion [13]. As opposed to this, ambient air is used to gradually cool crystalline material known as air-cooled slag (ACS) [14, 15]. Rapid cooling of iron slag

✉ Mohamed A. Ali
Mohamed.ahmed_ali@buc.edu.eg

Mohamed Heikal
mohamed.heikal@fsc.bu.edu.eg

[1] Chemistry Department, Faculty of Science, Benha University, Benha, Egypt

[2] School of Biotechnology, Badr University in Cairo (BUC), Badr City 11829, Cairo, Egypt

[3] Chemical Engineering Department, The Higher Institute of Engineering, El-Shorouk Academy, Shorouk City, Cairo, Egypt

with air is responsible for glassy or crystalline pellets known as pelletized blast-furnace slags (PBF) [6]. The World Steel Association estimates that about 90% of all by-products by weight is produced globally of steel slag because the iron and steel industry is one of the most energy and resource-intensive industries that contribute to greenhouse gas emissions [16]. The recycling of its waste, which is in line with the principle of the circular economy, has a significant environmental and economic impact. Iron slag has been extensively researched particularly for use in the production of building materials. One sink that is occasionally used to accommodate ACS is the construction industry by incorporating this by-product in concrete, building bricks, road construction etc. [17–23]. On the other hand, due to its vitreous structure, GBFS is frequently utilized as SCM throughout the world. In the presence of a suitable activator, it exhibits both cementitious behaviour and pozzolanic properties [24]. In this respect, [25, 26] showed that replacing cement partially with GBFS in concrete mix affects positively its workability. While Lee et.al [9] found that using GBFS elongates both the initial and final setting times and [9, 25, 27] noticed slow mechanical strength development at an early age. The results obtained by [25, 27–30] revealed that the compressive strength at later age exceeds that of free slag concrete. This improvement in mechanical properties is due to the high glass content of GBFS which increase pozzolanic activity. The partial replacement of cement by GBFS in concrete mix improves its durability against Cl^- attack [31]. They also recommended further testing on Cl^- and SO_4^{2-} attacks for longer times. Much more recently, [32] noted that the replacement of up to 70% of the cement with IGBFS improves the heat resistance for blended cement paste. Finally, a composite cement was employed to replace cement to utilize most industrial by-products; this improved the concrete's strength and/or lifespan [33, 34]. A combination of steel slag and IGBFS up to 40% was optimal, resulting in comparable compressive strength and denser structures, while also reducing environmental impacts [35]. With the directives of the Egyptian government to benefit from industrial by-products by reusing or recycling them in the interest of the environment and the economy, we decided to prepare a composite cement by mixing two types of by-products, IGBFS and ACS, to maximize environmental and economic benefits. Up to 180 days of hydration, the physicomechanical properties of the hardened cement pastes were investigated. Seawater attack and fire resistance are also examined.

Starting materials and their characterization

Tap water was utilized to mix and cure all cement pastes, and Suez Gulf seawater, which had sulphate and chloride concentrations of 8786 ppm and 12,543 ppm, respectively, was used as an aggressive medium to cure all specimens and study sulphate attack. Ordinary Portland cement (OPC) from the Suez Cement Company, the Iron Steel Company provided the air-cooled slag (ACS), Helwan, Egypt, and the IGBFS is supplied by (Kokan Mining Co. LTD, Japan). A laboratory steel ball mill with (a 5 kg) capacity is used to grind the slag into a fine powder. The specific surface area was calculated with the Blaine air-permeability device following the ASTM method [36]. The XRF analysis and the Blaine surface area of utilized materials are displayed in Table 1. Figure 1 illustrates the phase composition of ACS as determined by the XRD technique. It shows that the ACS is entirely crystalline phases (quartz (Q) and akermanite (A)). The IGBFS is typically almost entirely vitreous, with an amorphous hump typical of glass structure at 20 and 38 $2\theta^o$ attributed to the amorphous glassy component consistent with the network-forming oxides SiO_2 and Al_2O_3 making up the amorphous phase.

The OPC used in this study consists of four main phases with the following composition: Alite = 52.0%, belite = 19.20%, C_3A = 8.80% and C_4AF = 11.08%. XRD of IGBFS is seen in Fig. 1.

Experimental method

The IGBFS and ACS were finely processed using a laboratory steel ball mill with a 5 kg capacity after being crushed by a jaw crusher. Numerous specimens are created by mixing varying concentrations of IGBFS and ACS with a consistent quantity of OPC (30%). The mixes were denoted as A1, B1, B2, and B3 as shown in Table 2. The prepared mixes were mechanically combined for 1 h in a porcelain ball mill to achieve total homogeneity, and then tap water was used to hydrate the cement pastes. According to ASTM specifications, the water of consistency and setting times

Table 1 Chemical analysis (XRF), and the specific surface areas of utilized materials (wt %)

Item	IGBFS	OPC	ACS
SiO_2	37.48	20.51	40.78
Al_2O_3	12.86	5.07	10.95
Fe_2O_3	0.40	4.39	1.70
CaO	37.70	62.21	35.22
MgO	2.45	2.00	4.10
Na_2O	1.84	0.23	1.91
K_2O	0.93	0.29	0.58
BaO	5.31	0.00	0.0
SO_3	0.01	2.25	0.16
S^{2-}	0.75	0.0	0.0
L.O.I	0.00	2.40	0.0
Specific surface area (cm^2/g)	4300	3050	4000

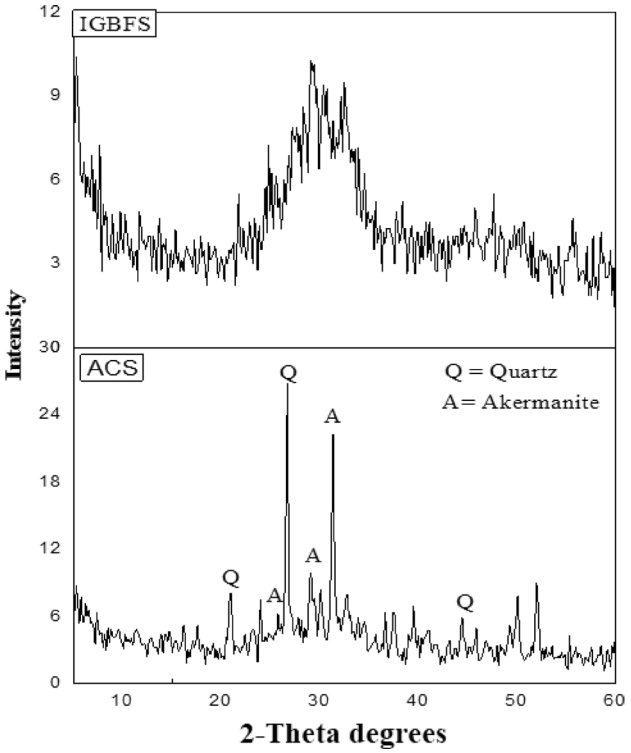

Fig. 1 XRD pattern of ACS and IGBFS

Table 2 The mix proportions for blended cement pastes, wt %

Mix No	OPC	IGBFS	ACS
A1	30	70	0.0
B1	30	60	10
B2	30	50	20
B3	30	40	30

for each combination were determined [37]. Stainless steel ($2.54 \times 2.54 \times 2.54$ cm^3) cubic molds were used for casting the cement pastes. The molds were then cured for the first 24 h in a humidity chamber with 100% relative humidity and a constant temperature of 25 °C. The molds were removed, and after that, they were submerged in water for the specified amount of time 3, 7, 28, 90, and/or 180 days. After any period of hydration, bulk density and total porosity were assessed as mentioned [38]. Chemically combined water content was assessed based on ignited weight loss [39, 40]**.** Ammonium acetate was used in a method to calculate the free lime content (FL.%) [41, 42]. As per ASTM (C-150) [43], compressive strength was assessed. The specimens underwent fire resistance testing after being cured solely in tap water for 28 days and dried at 105 °C for 24 h. They were thermally treated at a rate of 10 °C/min and held at a steady temperature for two hours at a maximum temperature of 800 °C to ensure consistency [44]. The paste specimens were subjected to temperatures of 25 °C, 250 °C, 450 °C, 600 °C, and 800 °C for a duration of 2 h, and then allowed to cool down to room temperature inside the furnace switched off. They were then covered with plastic film and placed in a desiccator to eliminate any potential moisture or carbonization effects. A set of four chips collected for each mix composition fired at appropriate temperature were immersed in kerosene for 24 h. The specimens were then the bulk density and total porosity were calculated using the density of kerosene (0.8 g/cm^3). To test the aggressive media's resistance for some selected specimens (A1, B1, B3), specimens were first cured under tap water for 28 days (zero time), then cured under seawater at 0, 1, 3, 6, and 12 months, respectively. Chemical composition of seawater is given in Table 3. The variations in compressive strength, bulk density, total porosity, combined water, and free lime contents for the immersed samples up to 1 year in Suez Gulf saltwater. The seawater from Suez Gulf as an aggressive medium was renewed every month with fresh seawater to attain the seawater nearly constant. After compressive strength test, samples were crushed and the hydration stopped using methanol/acetone/diethyl ether, followed by drying at 75 °C for 1 h [38, 39]. Some chosen hydrated samples were examined using differential thermal analysis (DTA/TGA), and differential scanning calorimetry (DSC) to confirm the mechanism anticipated by the chemical and mechanical testing. On choosing the hydrated and burnt cement pastes, X-ray diffraction method (XRD) testing was conducted. To provide further details on the hydrated products, infrared spectra were performed on a chosen paste.

Results and interpretation

Standard water of consistency and setting times

Figure 2 shows a graphic representation of the water of consistency and initial and final setting times of composite cement pastes prepared from IGBFS and ACS as a function of mix composition. With the replacement of IGBFS with ACS, it is evident that the required water of standard consistency was slightly reduced. But when ACS concentration

Table 3 The ion concentration of Suez Gulf seawater

Ions	Ca^{2+}	Mg^{2+}	Cl^-	SO_4^{2-}	Na^+	T.D.S*
Concentration, ppm	425	837	12,543	8786	14,522	35,939

**T.D.S* Total dissolved solids

increases, both initial and final setting times were increased up to 10–20 wt% ACS, which gives small elongation. At 30 wt% the setting time is elongated at a higher rate than at 10–20 wt. %. As a result of the greater concentration of ACS, there is a somewhat pozzolanic reaction and a consequent decrease in the hydration products of C-S-H, C-A-H, and C-A-S-H. For cement pastes to be set, these phases are necessary.

Chemically combined water contents

Figure 3 shows the change in chemically combined water contents with the time of curing in. The results reveal that the combined water content rises with curing time where cement continues to hydrate and more C-S-H, C-A-H, and C-A-S-H are formed. Also, the chemically combined water content reflects the high extent of hydration reaction of OPC cement-containing phases (β-C_2S and C_3S) to generate C-S-H and $Ca(OH)_2$ (CH), and CH serves as a pozzolanic activator. On the other hand, the accumulated hydration products and hence the combined water likewise drop as the IGBFS declines at the expense of ACS. Mix B3, which consists of 40% IGBFS and 30% ACS, exhibits a slower hydration rate when compared to the other mixtures. This can be primarily attributed to the slower hydration rate of ACS as compared to Portland cement. Additionally, the combined water content in pozzolanic cement pastes is lower than that in OPC paste hydration [45].

Free lime contents

Free lime contents of all specimens are varied with curing time as described in Fig. 4. The results demonstrate that the curing time affects free lime content negatively, this is due to the persistence of the pozzolanic reaction between IGBFS and the produced CH during the cement hydration [46]. Free lime content declines when ACS is substituted for

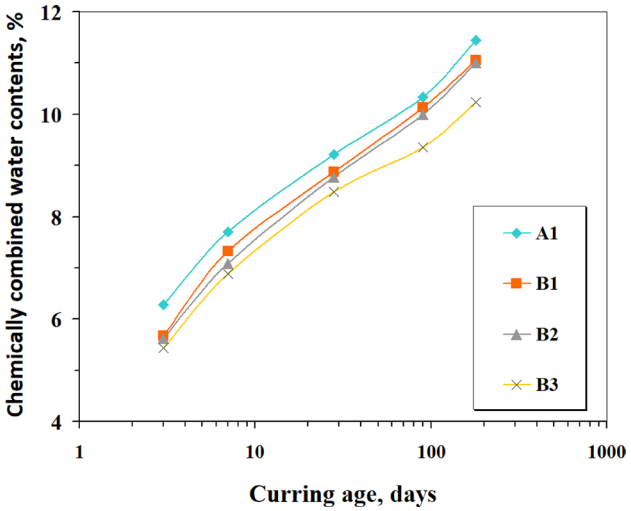

Fig. 3 Effect of replacement of IGBFS with ACS on chemical combined water of hydrated IGBFS-rich cement pastes up to 180 days

IGBFS; for example, cement paste with 30 weight percent ACS gives the highest values of free lime during the entire curing time of up to 180 days. Residual $Ca(OH)_2$ diminishes by the amount of ACS decreasing at the expense of IGBFS. This is mostly because IGBFS has a greater pozzolanic activity level. It is also obvious that free lime consumption increases with curing age, which is mainly because there is more pozzolanic activity at a later age than at an early age.

Bulk density

Figure 5 illustrates the variation in the bulk density with a curing time of up to 180 days. The bulk density of cement pastes cured up to 180 days is reduced when a 10-weight percent of IGBFS is replaced with ACS. This is primarily because IGBFS, which has a high pozzolanic response, has

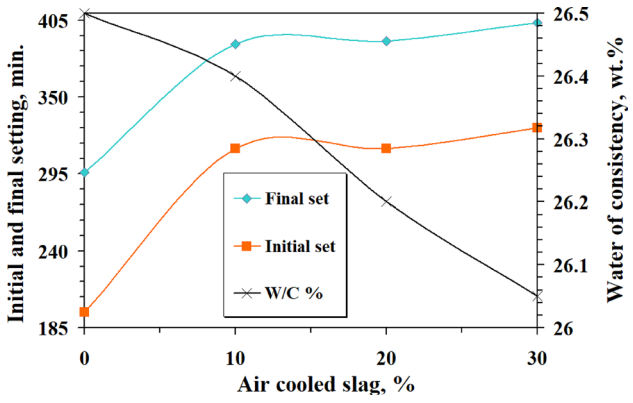

Fig. 2 Effect of replacement of IGBFS with ACS on water of consistency, initial and final setting times of IGBFS rich cement pastes

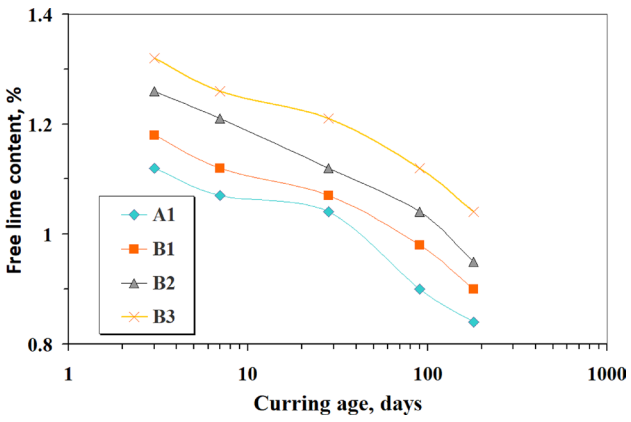

Fig. 4 Effect of replacement of IGBFS with ACS on the total free lime content of hydrated IGBFS-rich cement paste up to 180 days

better hydraulic characteristics than ACS, which has weak hydraulic qualities. The equivalent bulk density is raised to 180 days of hydration when IGBFS is substituted with ACS at 20 and 30 wt%, this is mostly caused by the fact that ACS has a larger bulk density than IGBFS. Because a portion of the accessible pores is filled with cement paste during the curing process, the overall volume of the pores is reduced, which increases the bulk density of the solid materials [47].

Total porosity

Figure 6 illustrates the change in total porosity with a time of curing of up to 180 days for ACS and IGBFS cement paste. It is evident that, up to 180 days, the total porosity of IGBFS without ACS provides practically the lowest total porosity of any composite cement paste. Conversely, composite cement pastes with 10 and 20 wt% ACS produce almost the same total porosity and are higher than those with 30% ACS and without ACS. Cement paste composed of 30% ACS with 40% IGBFS with only 30 wt% OPC shows an intermediate value between the pozzolanic cement paste with 70% IGBFS and the composite cement pastes containing 10–20% ACS. The figure also shows a sharp drop in total porosity from 90 up to 180 days. This is mainly because composite cement pastes exhibit greater pozzolanic activity at later ages [48].

Compressive strength

The results presented in Fig. 7 showed that the mechanical compressive strength was positively affected by curing time for all specimens under study. B1 achieved the highest compressive strength of all since 10% ACS service as a nucleating agent which stimulated the hydration rate which is positively reflected in the compressive strength. Cement pastes without ACS and 70 wt% IGBFS give lower compressive strength than that containing 60 wt% IGBFS and

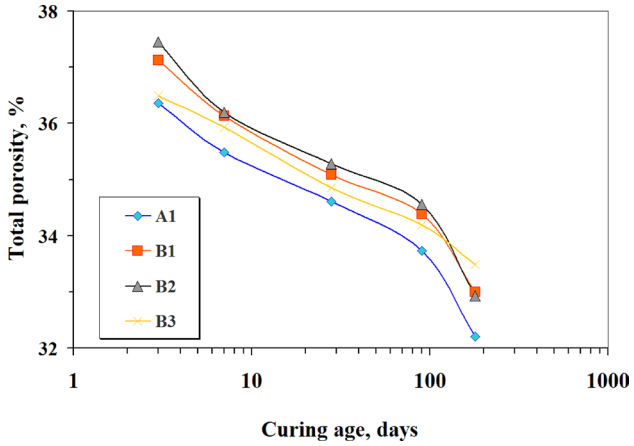

Fig. 6 Effect of replacement of IGBFS with ACS on the total porosity of hydrated IGBFS-rich cement paste up to 180 days

10 wt% ACS as previously discussed which ACS acts as nucleating sites. With an increase in ACS content of more than 10%, the compressive strength is negatively affected. These cement pastes are blended since ACS has lower hydraulic material, which affects the strength negatively. All specimens behaved in the same way, as the compressive strength increased quietly in the first days, unlike what happens after three months and up to 6 months. We also notice a sharp increase in strength, this is due to the recent growth of pozzolanic activity. Also, the variation in the compressive strength with the chemical water content is presented in Fig. 8, and a mathematical linear equation has been established with a goodness coefficient greater than 0.75. These findings are in good accord with those of [49].

The relationship between the compressive strength and bound water content in hydrated cement is not necessarily linear. This relationship depends on a variety of factors, such as the composition of the cement, the curing conditions,

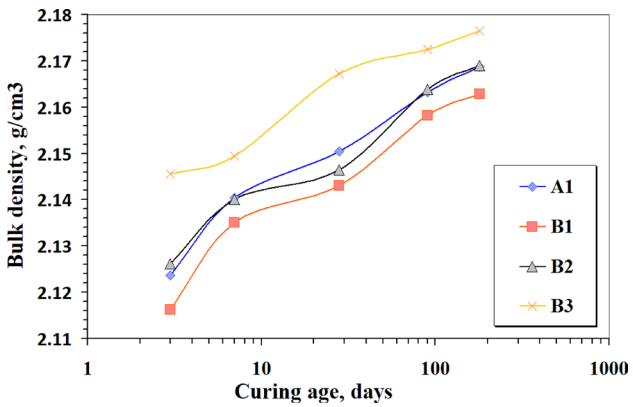

Fig. 5 Effect of replacement of IGBFS with ACS on the bulk density of hydrated IGBFS-rich cement paste up to 180 days

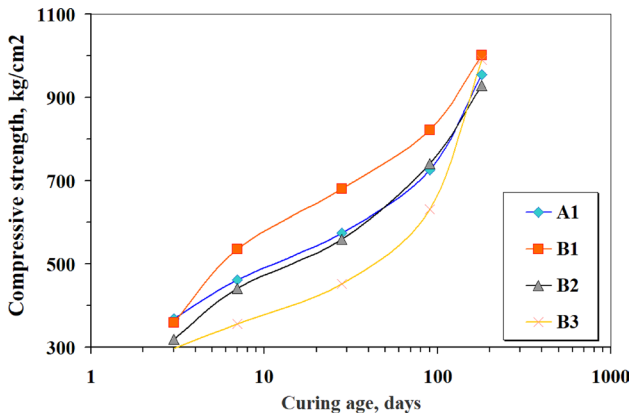

Fig. 7 Effect of replacement of IGBFS with ACS on the compressive strength of hydrated IGBFS rich cement paste up to 180 days

and the testing method used. In some cases, it observed a linear relationship between compressive strength and bound water content in hydrated cement [49–51]. However, other studies have found non-linear relationships or more complex relationships between these two factors. Scrivener *et. al.* discussed the complexities of the hydration process in OPC and its influence on compressive strength. It emphasizes the non-linear relationship between bound water content and strength development [52].

FT-IR spectroscopy

Figure 9 shows the FT-IR patterns of hydration products of IGBFS and ACS -cement pastes (A1 and B3) after 180 days. Absorption bands at 3448–3456 cm^{-1} and 1647–1653 cm^{-1} are related to stretching and bending vibration of O–H groups of H:OH, respectively. Absorption bands of water are due to the lattice H_2O of the hydrated C-S–H, C-A-H as well as C-A-S–H. [53, 54]. The band at 1633 cm^{-1} decreases in B3 due to the decrease of combined water with ACS. The band at 1433 cm^{-1} is attributed to the presence of calcite, possibly formed due to carbonation of the pastes [55, 56]. The intensity of the band at 976 cm^{-1} is due to Si–O stretching vibration of C-S-H [57]. Increases in A1 (indicating the increase of C-S-H). This is observed in the higher values of compressive strength of A1 than B3 at 180 days.

Thermogravimetric analysis (DTA/TGA)

Figure 10 illustrates the DTA thermograms of mixes A1 and B3 at 180 days. The dehydration of water and combined free from C-S-H within the hydrated cement matrix causes endotherms to occur at 70–120 °C [58]. The endothermic peaks associated with C-A-H and C-A-S-H occur at 269, and

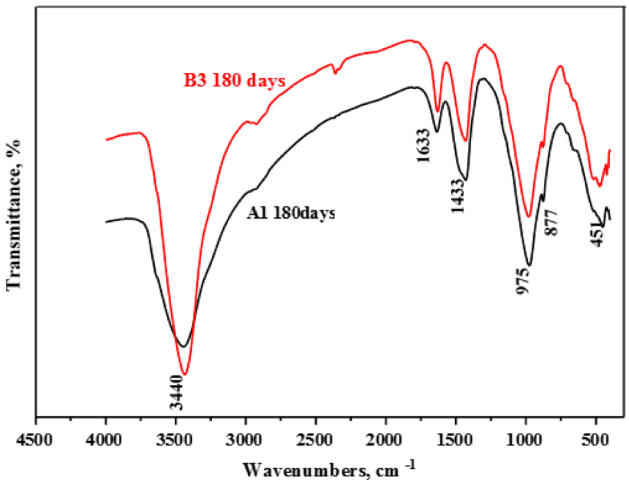

Fig. 9 FT-IR spectroscopy of A1 and B3 mixes cured up to 180 days

345 °C [59]. The endothermic peaks around 664–758 °C, are related to the breakdown of carbonate, hydrated aluminates, and the final phase of C-S–H decomposition [60]. The exothermic peak at 845–900 °C is caused by wollastonite recrystallizing [61]. Additionally, the endothermic peaks at the low-temperature range due to the decomposition of hydration products increase with IGBFS content. This means that mix A1 with 70 wt% IGBFS gives better hydration product values as seen from the peak area of the hydrated pastes. As the ACS content increases at the expense of IGBFS the hydration products decrease. This is mainly due to the higher degree of hydration of IGBFS in comparison to ACS. The breakdown of well-crystallized $CaCO_3$ is what causes the endothermic peak at 878 °C. The ACS contains a small endothermic peak in the range of 345 °C due to the decomposition of brucite $Mg(OH)_2$. The dehydroxylation of portlandite is responsible for the endothermic peak in the

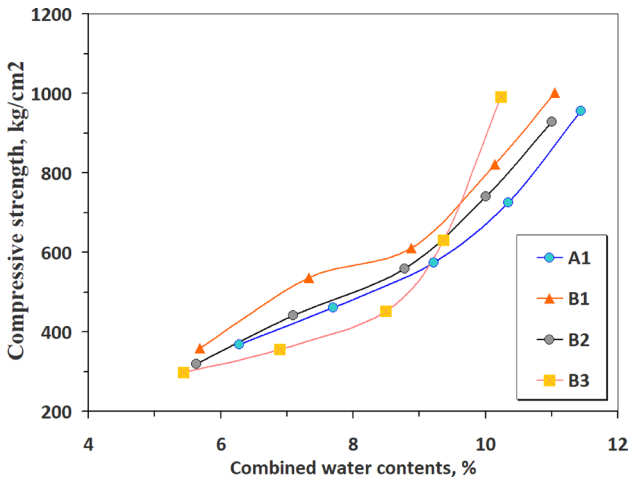

Fig. 8 Compressive strength of Imported IGBFS and ACS rich cement pastes with combined water

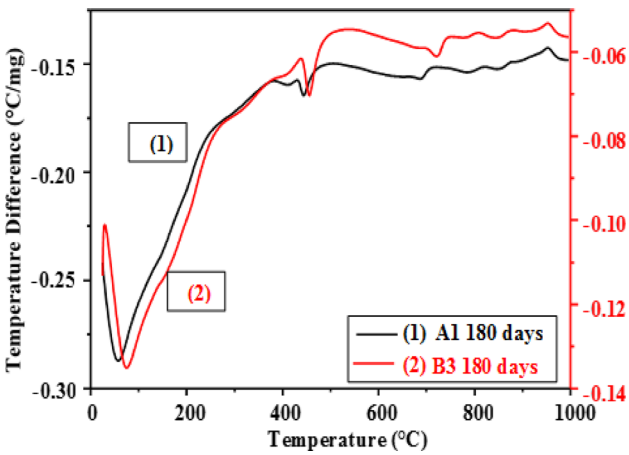

Fig. 10 The DTA thermograms of hydrated Imported IGBFS and ACS rich cement paste of mixes A1 and B3 at 180-days

395–450 °C range. Due to the strong pozzolanic activity of IGBFS in comparison to ACS, it is obvious that the peak of portlandite in the case of A1 is more intense than that of B3. As a result, B3 paste has more portlandite than A1 paste.

Figure 11 illustrates the thermogravimetric analysis (TGA) of hydrated A1 and B3 cement pastes for up to 180 days. TGA losses of A1, and B3 because hydration products are decomposed up to 250 °C are 8.489 and 7.795 wt% for A1 and B3, respectively. On the other hand, the TGA losses due to the dehydroxylation of portlandite are 3.318 and 4.016 wt% for A1 and B3, respectively. The last decomposition of the CO_3^{2-} is 2.622 and 3.105 wt% for A1 and B3, respectively. The cement paste A1 is more hydraulic than B3. This is mainly due to the incorporation of ACS (B3) instead of IGBFS (A1). The IGBFS has a pozzolanic reaction whereas ACS is less hydraulic material. Cement paste's combined water content is 11.113 and 12.505 wt% of B3 and A1.

It is obvious that IGBFS results in higher combined water content. The combined water as determined by the chemical method includes the loss of both $Ca(OH)_2$ and $CaCO_3$. The IGBFS is more hydraulic than ACS and these values are in according with the determined values of combined water. Cement paste containing 70 wt% IGBFS gives weight loss of 8.489, 12.505, and 15.51 wt% whereas cement paste with 40% IGBFS and 30% ACS shows 7.795, 11.113, and 13.735 wt. %. This means the cement with higher content of IGBFS is more hydraulic.

Effect of firing temperature

Weight loss

A graphical plot of the weight loss of hardened specimens (A1, B1, B2 and B3) varied with the thermal treatment temperatures up to 800 °C, is presented in Fig. 12. Because of the breakdown of some hydration products, weight loss typically increases with treatment temperature for all cement pastes [10]. Below 105 °C, the free water was eliminated, and below 200 °C, calcium silicate, aluminate, sulphoaluminate, and aluminum–silicate hydrate partially decomposed. At 200–250 °C, gehlenite hydrate (C_2ASH_8) phase starts to break down. Between 420 and 520 °C, $Ca(OH)_2$ underwent dehydroxylation [62]. The decomposition of C-S-H, C-A-H, calcium sulphoaluminate hydrates, gehlenite hydrate, and $Ca(OH)_2$ causes the weight loss to increase up to 800 °C [10, 63]. It has been demonstrated that up to 800 °C, A1 loses more weight than B1, B2, and B3. The reduction of mixing water, which results in a drop in the quantities of free and chemically mixed water, may be responsible for the decreased weight loss of B1, B2, and B3. Additionally, the rate of hydration and subsequent weight loss of cement pastes are both reduced when ACS is added in place of IGBFS.

Bulk density

Figure 13 illustrates the relationship between the bulk density of treated pozzolanic cement pastes with varying IGBFS and ACS dosages and the thermal treatment temperature up to 800 °C. It is evident that treatment temperatures up to 250 °C, result in a decrease in bulk density. At all treatment temperatures, cement pastes without ACS had the lowest bulk densities. The breakdown of some hydration products causes the bulk density to decrease, but the ACS has a higher specific gravity than IGBFS, which tends to increase the bulk density. The elimination of free or adsorbed as well as bound water of C-S-H or C-A-H has taken place. There are three phases involved in changing the bulk density of

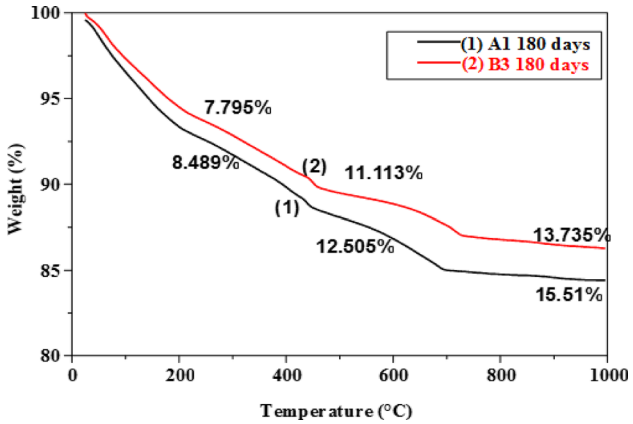

Fig. 11 The TGA thermograms of hydrated Imported IGBFS and ACS rich cement pastes of A1 and B3 at 180-days

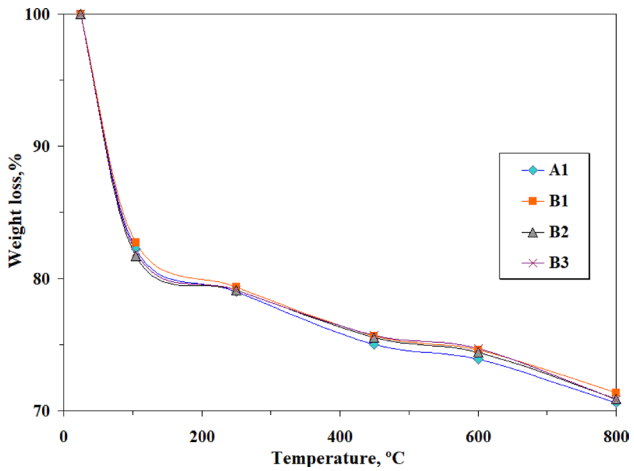

Fig. 12 Effect of replacement of IGBFS with ACS on the weight loss of hydrated IGBFS-rich cement paste at different temperatures

variously treated cement pastes. The apparent density typically declines with treatment temperature up to 250 °C (first step). The density is virtually the same in the second step, between 250 and 400 °C. For all pozzolanic cement pastes, a rise in density is observed during the third step (from 400 to 800 °C). In comparison to other pozzolanic cement pastes, B3 rich in ACS cement paste has a higher apparent density. This is mostly because of ACS's denser structure and higher specific gravity compared to GBFS.

Total porosity

A graphical plot of the porosity of hardened specimens (A1, B1, B2 and B3) varied with the treatment temperature up to 800 °C, is presented in Fig. 14. The breakdown of hydration products $Ca(OH)_2$ and $CaCO_3$ causes the total porosity typically increases with treatment temperature from 400 to 800 °C for all cement pastes [64]. The internal cracks growth in B2 and B3 leads to a total porosity rise up to 800 °C. In addition, increasing the percentage of ACS negatively affects the hydration rate, which in turn increases the porosity. It can be concluded that mix A1 (30% OPC with 70% IGBFS) gives lower porosity in comparison to others because of product accumulation growth in its open pores.

Compressive strength

Figure 15 illustrates the compressive strength as a function of treated temperature from 105 °C up to 800 °C. Compressive strength can be found to rise with temperature up to 250 °C before decreasing up to 800 °C. The increase in cement paste hydration products and the pozzolanic reaction of IGBFS with CH to produce additional amounts of C-S-H with a low Ca/Si ratio and high strength are both responsible

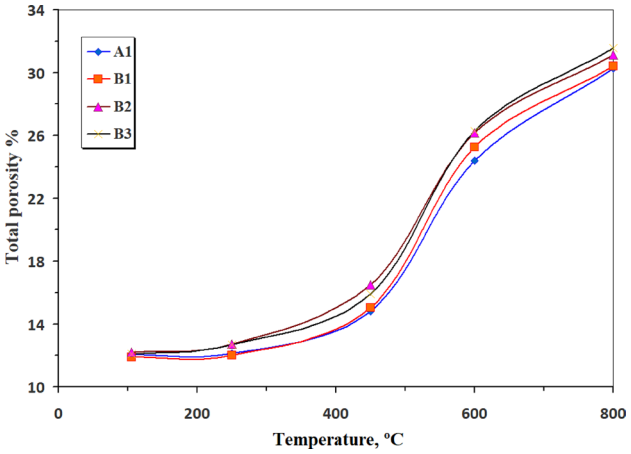

Fig. 14 Effect of replacement of IGBFS with ACS on the total porosity of hydrated IGBFS rich cement paste at different temperatures

for the increase in compressive strength up to 250 °C [65]. This is also a result of the internal and self-autoclaving action, in which steam accumulates due to the removal of capillary, adsorbed, and bound water at high temperatures. This increases the pressure of steam, which speeds up the hydration of anhydrous cement paste grains to form dense-microstructure matrixes [66]. At 800 °C, the dissociation of cementing ingredients and swelling of the water layer in cement pastes cause the compressive strength to diminish [67]. Additionally, the coarsening of the pore size distribution causes an increase in porosity [65]. The A1 (70 wt% IGBFS) is more heat resistant than the other specimens at all temperatures. This is because increased amounts of calcium silicate, aluminate, and aluminum silicate hydrates are produced as a result of the reaction between released lime and IGBFS. The compressive strength is increased by these

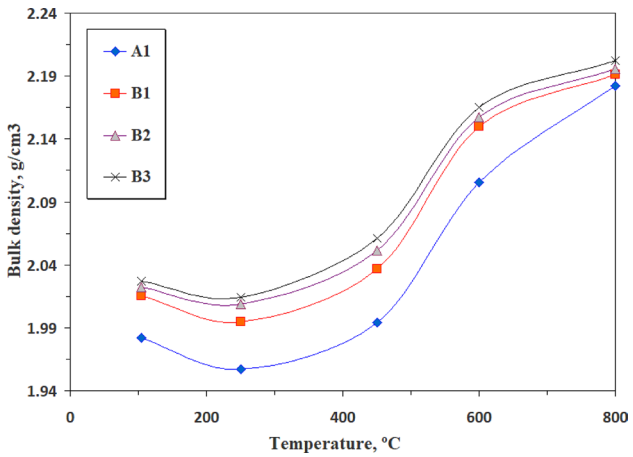

Fig. 13 Effect of replacement of IGBFS with ACS on the bulk density of hydrated IGBFS-rich cement paste at different temperatures

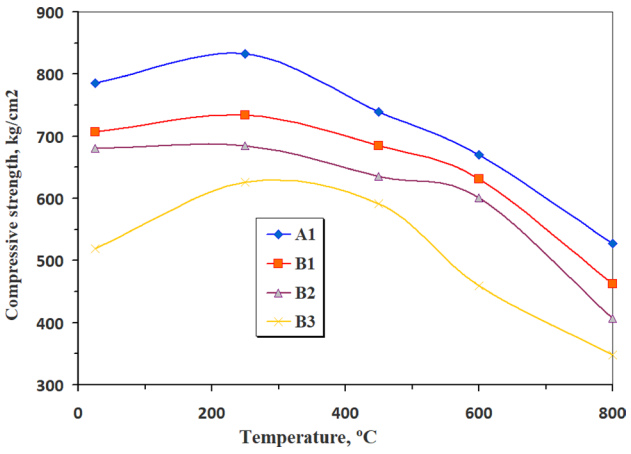

Fig. 15 Effect of replacement of IGBFS with ACS on the compressive strength of hydrated IGBFS-rich cement paste at different temperatures

hydrates that have been deposited within the pore system. The compressive strength of thermally treated cement pastes tends to decrease when equal amounts of IGBFS are substituted with ACS. The compressive strength of B1 cement paste is almost identical to that of A1, although at lower values. Additionally, the compressive strength rises with ACS content i.e., 30% up to 250 °C before declining. The thermal resistance of ACS up to 300 °C may be to blame for this rise. The slow rate of hydration of B3 at 105 °C explains the lower strength.

The visual inspection of pozzolanic cement thermally treated at 600–800 °C is shown in Fig. 16. The surface cracks appeared at 600 °C, which propagated at 800 °C. These cracks diminished with A1 mix. Hence, the pozzolanic cement pastes, A1 mix, improve the thermally treatment resistance.

Effect of seawater attack

Chemically combined water content

Figure 17 illustrates the combined water content of IGBFS and ACS cement pastes submerged in seawater. The combined water content increases with an immersing period for A1 cement paste, and increases up to 6 months for cement pastes B1 and B3 containing ACS with IGBFS then decreases gradually up to 12 months. The increase of combined water of A1 mix containing 70% IGBFS up to one year of seawater immersion primarily as a result of the high pozzolanic nature of IGBFS. On the other side, the pastes containing 10 and 30 wt% ACS show lower water contents than A1 up to 1 year. The combined water content also drops as ACS increases because of ACS inert nature. The decrease in combined water contents after 6 months in seawater may be due to silicate polymerization with low water content.

Free lime content

Figure 18 shows a graphic description of the values of free lime of various cement pastes immersed in seawater for a year. According to the results, the free lime contents of all cement pastes decrease gradually up to one year of immersion in seawater; this results from IGBFS- pozzolanic reaction as activated by lime leading to the extra-formation of C-S–H and C-A-S-H [46]. As the amount of IGBFS slag increases the free lime content decreases due to the high pozzolanic properties of GBFS. Because ACS has

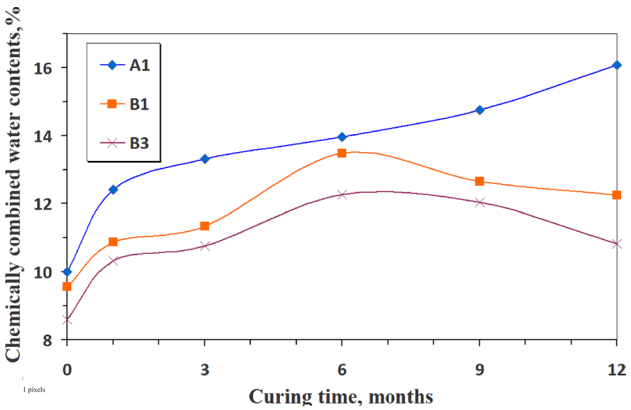

Fig. 17 Effect of replacement of IGBFS with ACS on the chemically combined water of hydrated IGBFS-rich cement paste immersed in seawater up to a year

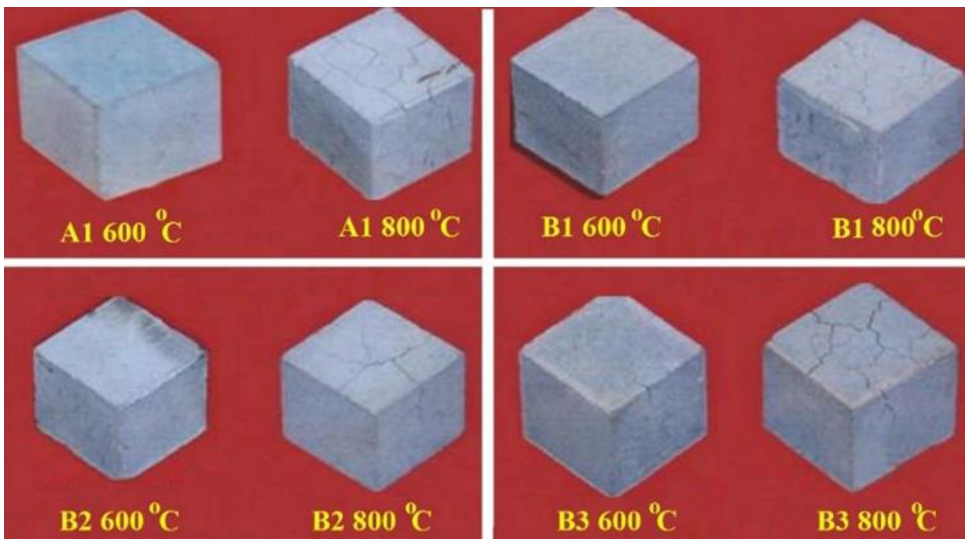

Fig. 16 The visual inspection of pozzolanic cement thermally treated at 600 up to 800℃

a low pozzolanic ability to react with residual free lime, the amount of free lime in cement pastes containing ACS increases.

Bulk density

The variation in bulk density of the hardened specimens immersed in seawater against curing age is plotted in Fig. 19. According to the results, the cement is stimulated by Cl^- and SO_4^{2-} ions in seawater to produce wet hydrated products that fill some open pores, increasing the bulk density over a year of immersion in seawater. The bulk density of the specimens, on the other hand, improves when the ACS content rises. This suggests that ACS anhydrous grains have higher specific gravities than IGBFS grains.

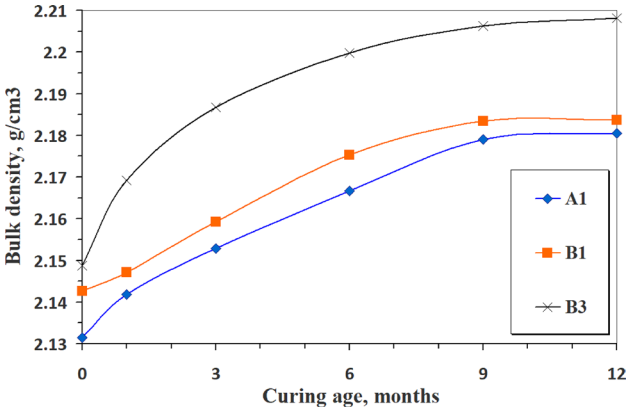

Fig. 19 Effect of replacement of IGBFS with ACS on the bulk density of hydrated IGBFS-rich cement pastes immersed in seawater up to a year

Total porosity

The total porosity of the hardened pastes immersed in seawater for 1, 3, 6, 9 and 12 months are shown in Fig. 20. Owing to the precipitation of hydrated products into the accessible pores of cement pastes [48], the total porosity of all specimens steadily decreases with immersion time. The total porosity of the immersed specimens is reduced when IGBFS is substituted with ACS due to the ACS nucleating effect, in addition to the role of (Cl^- and SO_4^{2-}) which accelerated the cement hydration.

Compressive strength

The compressive strength of the specimens immersed in seawater for a year is plotted in Fig. 21. The results indicated that cement pastes strength improved for up to six months before decreasing for up to a year. The fundamental reason for this is because the pastes activation with Cl^- and SO_4^{2-} in seawater produced additional hydration products, particularly hydrated calcium silicate hydrates which affect the strength positively. Since pozzolanic material and a nucleating agent are presented at the early 6 months of immersion, both activated the hydration of IGBFS-rich cement pastes containing ACS, which results in an increase in compressive strength of B1 at early and later ages of immersion. Due to the larger concentration of ACS with poor hydraulic characteristics, B3 has a lower compressive strength. In general, the acceleration action of both sodium and magnesium salts i.e. Cl^- and SO_4^{2-} on cement pastes is the major cause of the strength improvement up to six months. A portion of Mg^{2+} is diffused and adsorbed into the C-S–H particles which stimulate its crystallization and lead to strength improvement. As a result of this activation, calcium silicate, chloroaluminate, and sulphoaluminate hydrates (ettringite minerals) are produced. After six months

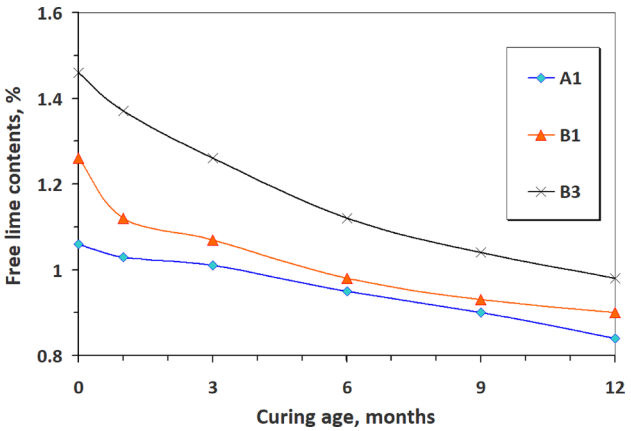

Fig. 18 Effect of replacement of IGBFS with ACS on the free lime of hydrated IGBFS-rich cement pastes immersed in seawater up to a year

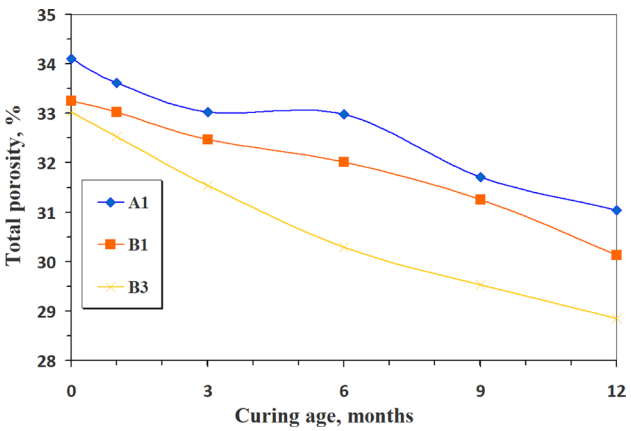

Fig. 20 Effect of replacement of IGBFS with ACS on the total porosity of hydrated IGBFS-rich cement pastes immersed in seawater up to a year

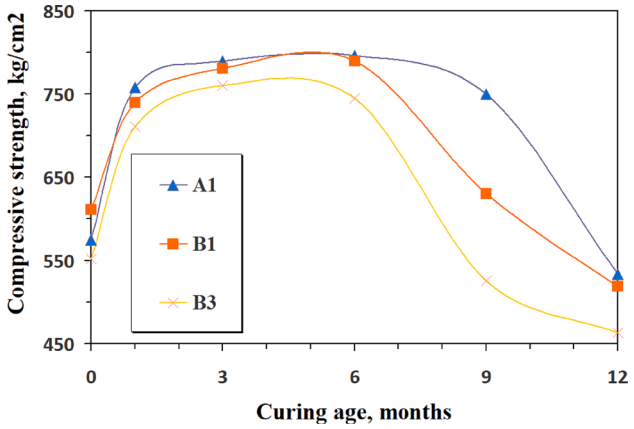

Fig. 21 Effect of replacement of IGBFS with ACS on the compressive strength of hydrated IGBFS-rich cement pastes immersed in seawater up to a year

up to 12 months in seawater, the compressive strength begins to diminish as more calcium chloroaluminate hydrates and ettringite forms as represented in Fig. 21. The visual photos of pozzolanic cement pastes of A1, B1 and B3 cured at 6 and 12 months are given in Fig. 22.

FT-IR spectroscopy

The reduced intensity of the portlandite band at 3454 cm^{-1} at 12 months is shown in Fig. 23 which displays the FT-IR spectra of A1 at 0, 6 and 12 months of immersion in seawater. This is explained by the IGBFS's pozzolanic reaction with portlandite involved in cement hydration. CH is converted into $CaSO_4.2H_2O$ and $Mg(OH)_2$ by the acidic action of $MgSO_4$ in seawater. A further portion of $Ca(OH)_2$ is also broken down by $MgCl_2$ to produce $Mg(OH)_2$.

XRD analysis

The XRD patterns of A1 at 0, 6, and 12 months are presented in Fig. 24. The hydration process causes the concentrations of $Ca(OH)_2$, $CaCO_3$, C-S–H, -C_2S, and C_3S to drop with time. 28-day immersion in tap water does not result in the formation of calcium chloroaluminate hydrate. On prolonged hydration, the intensity of the peak corresponding to the calcium chloroaluminate hydrate increases. Additionally, due to the pozzolanic reaction of IGBFS with portlandite, CH is entirely consumed after 6 months of immersion. Until a year, anhydrous phases such β-C_2S and C_3S are still present.

Thermal analysis of cement pastes immersed in seawater

The effect of seawater attack on the hydration products of IGBFS cement pastes immersed in seawater for up to one year can be studied with the aid of DTA Fig. 25. The thermograms indicate different endothermic peaks in addition to

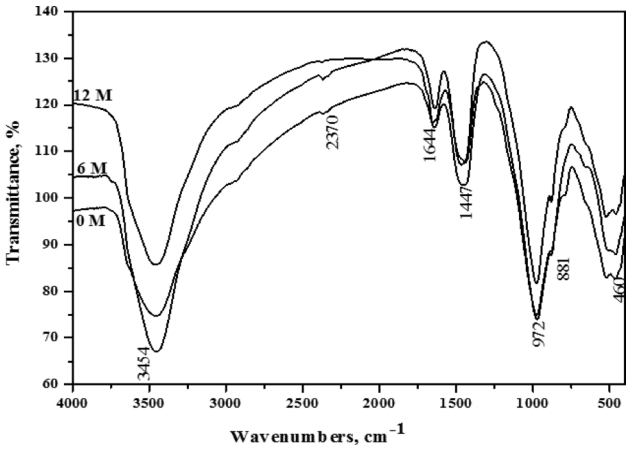

Fig. 23 FTIR spectroscopy of A1 (30% OPC + 70% IGBFS) immersed in seawater for 0, 6 and 12 months

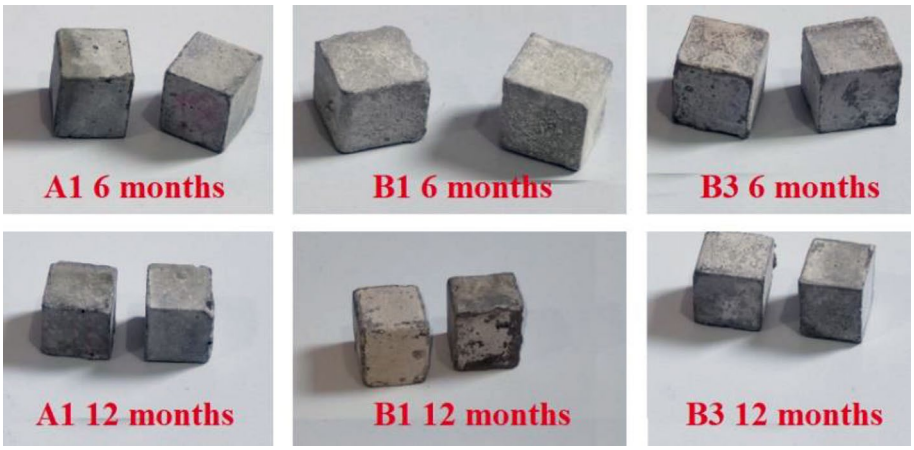

Fig. 22 The visual photos of pozzolanic cement pastes of A1, B1 and B3 cured at 6 and 12 months

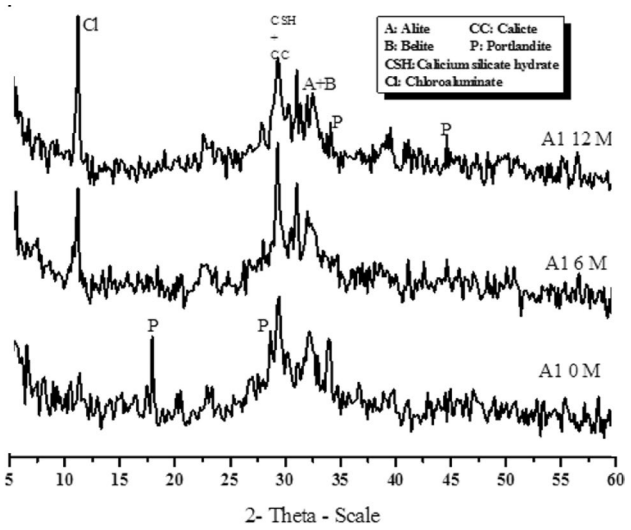

Fig. 24 XRD patterns of A1 at 0, 6 and 12 months under seawater

one exothermic peak at about 955 °C. The lower endotherms up to 300 °C are due to the decomposition of C-S-H, ettringite and calcium chloroaluminate hydrate. There are other three endothermic peaks at 316, 428 and 459 °C; which appear with the decomposition of C_2ASH_8, brucite and portlandite, respectively. Two endothermic peaks located in the range of 700–900 °C appear with calcination of the amorphous and crystalline calcium carbonate [68, 69]. The exothermic peak at 956 °C is characteristic of the C-S-H involved with the crystallization of monocalcium silicate $CaO.SiO_2$ (wollastonite).

The thermogram of mix A1 at zero time shows the C-S-H, AFt, C_2ASH_8 and hydro garnet series at 315 °C as represented in Fig. 25. There is a characteristic endothermic peak of $Ca(OH)_2$ and endothermic peaks of $CaCO_3$ in addition to an exothermic peak for the crystallization of wollastonite [70]. A1 at 6 months immersion in seawater gained the highest hydration products yield which reflects the ability of seawater to activate the hydration reaction to some extent at an earlier age. The amounts of chloroaluminate, sulphoaluminate. C-S-H and hydrogarnet hydrates series increase with the decrease of the endotherm of C-S-H as well as $Ca(OH)_2$ due to the reaction of $MgCl_2$ and $NaCl_2$ with $Ca(OH)_2$ to form brucite $Mg(OH)_2$, as small endotherm at 438 °C. As the immersing time increases the amounts of hydration products as well as the hydrogarnet and $Mg(OH)_2$ increase with the consumption of $Ca(OH)_2$. This is also a result of $Ca(OH)_2$ and chloride's reaction. The endothermic peaks due to the carbonation are also detected. The exothermic peak at 955 °C is also present, which is sharp at zero month (0 M) (in tap water). Then the intensity and the sharpness of the exothermic peak decrease. This is also a result of chloride or sulphate ions attacking C-S-H, as seen in the equation below.

$$3CaO.SiO_2.3H_2O + MgCl_2 \rightarrow Mg(OH)_2 + CaCl_2 + SiO_2gel$$

Therefore, the amount of C-S-H decreases with the $CaCl_2$ content because of the chloroaluminate hydrate growth. Hence, C-S-H decreases at later ages (12 months) as seen from the DTA thermograms.

Conclusion

1. When ACS was used in place of GBFS, the water consistency of cement pastes marginally decreased.

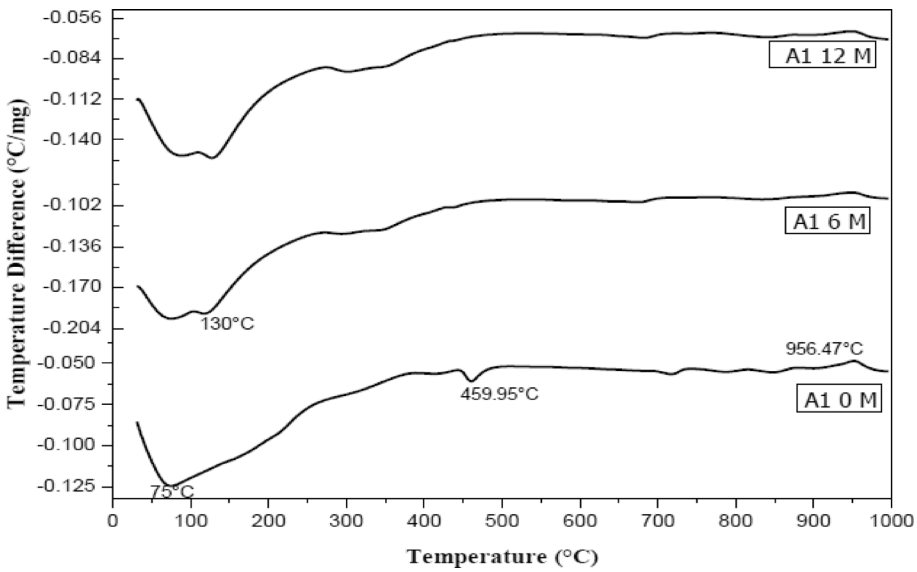

Fig. 25 DTA thermograms of A1 immersed in seawater for 0, 6 and 12 months

2. The initial, as well as final setting time, are prolonged with ACS content, 10–20 wt% ACS gained small elongation.
3. As the IGBFS decreases on the expense of ACS the accumulated hydration products and hence the combined water decreases and the free lime increases.
4. It is clear that the IGBFS is more hydraulic than ACS and these values are in according with the determined values of combined water.
5. All specimens gain compressive strength with curing age up to 180 days and that of 10% ACS show higher compressive strength than those containing 20–30 wt% and without ACS.
6. The incorporation of ACS at expense of IGBFS tends to increase the bulk density of thermally treated specimens. On the other side, the substitution of IGBFS with ACS decreases the compressive strength up to 800 °C.
7. The compressive strength improved for all specimens submerged in seawater at an earlier age and then decreases up to a year, the ACS-rich cement paste has the lower compressive strength. In contrast, a 7% reduction in the compressive strength is less than achieved at zero time by IGBFS-rich cement paste.

While this study examined cement pastes with a specific W/C ratio, further work is needed to determine the effects of W/C on the properties of these composite cements. Based on the promising results of this initial characterization, future studies will investigate composite slag cements over a range of W/C ratios. Optimizing both strength and workability properties through adjustments in W/C will be the focus of continued research in this area.

Authors contribution MH: supervision, data curation, visualization, validation, investigation, writing—reviewing and editing, MAA, SMI, HI: conceptualization, writing—original draft preparation, investigation, software, writing—reviewing and editing, and data curation, visualization.

Funding Open access funding provided by The Science, Technology & Innovation Funding Authority (STDF) in cooperation with The Egyptian Knowledge Bank (EKB).

Declarations

Institutional review board statement The study was conducted and approved according to the guidelines of the declaration of the ethical committee of the Faculty of Science, Benha University (BUFS-REC-2023-22 chm).

References

1. Pedraza J, Zimmermann A, Tobon J, Schomäcker R, Rojas N (2021) On the road to net zero-emission cement: integrated assessment of mineral carbonation of cement kiln dust. CHEM ENG J 408:127346. https://doi.org/10.1016/j.cej.2020.127346
2. Salas DA, Ramirez AD, Rodríguez CR, Petroche DM, Boero AJ, Duque-Rivera J (2016) Environmental impacts, life cycle assessment and potential improvement measures for cement production: a literature review. J CLEAN PROD 113:114–122. https://doi.org/10.1016/j.jclepro.2015.11.078
3. Saleh H, AL-Kahlidi M, Abulridha, HA, Banoon SR, Abdelzaher MA, (2021). Current situation and future prospects for plastic waste in maysan governorate: effects and treatment during the COVID-19 pandemic. Egypt J Chem, 64 (8), 4449–4460. doi: https://doi.org/10.21608/ejchem.2021.79255.3895
4. El-Kattan IM, Abdelzaher M, Farghali A (2020) Positive impact of ultra fine-ceramic waste on the physico-mechanical features and microstructure of white cement pastes composites. J Market Res 9(4):9395–9402. https://doi.org/10.1016/j.jmrt.2020.05.087
5. Tüfekçi M, Demirbaş A, Genc H (1997) Evaluation of steel furnace slags as cement additives. Cem Concr Res 27(11):1713–1717. https://doi.org/10.1016/S0008-8846(97)00158-0
6. EUROSLAG. (2018). The European Association Representing Metallurgical Slag Producers and Processors.
7. Perez-Garcia F, Parron-Rubio ME, Garcia-Manrique JM, Rubio-Cintas MD (2019) Study of the suitability of different types of slag and its influence on the quality of green grouts obtained by partial replacement of cement. Materials 12(7):1166
8. Luciano A, Reale P, Cutaia L, Carletti R, Pentassuglia R, Elmo G, Mancini G (2020) Resources optimization and sustainable waste management in construction chain in Italy: toward a resource efficiency plan. Waste and Biomass Valorization 11:5405–5417
9. Lee JY, Choi JS, Yuan TF, Yoon YS, Mitchell D (2019) Comparing Properties of concrete containing electric arc furnace slag and granulated blast furnace slag. Materials (Basel) 12(9):1371. https://doi.org/10.3390/ma12091371
10. Heikal M, Abd El Aleem S, Morsi W (2013) Characteristics of blended cements containing nano-silica. HBRC Journal 9(3):243–255
11. Aziz MA-E, Aleem SAE, Heikal M (2012) Physico-chemical and mechanical characteristics of pozzolanic cement pastes and mortars hydrated at different curing temperatures. Constr Build Mater 26(1):310–316
12. Siddique, R. (2007). Waste materials and by-products in concrete: Springer Science & Business Media.
13. Siddique R (2014) Utilization (recycling) of iron and steel industry by-product (GGBS) in concrete: strength and durability properties. J Mater Cycles Waste Manage 16:460–467
14. Vasanthi P (2014) Flexural behaviour of reinforced concrete slabs using steel slag as coarse aggregate replacement. Int J Res Eng Technol 3:141–146
15. Thangaselvi K (2015) Strength and durability of concrete using steel slag as a partial replacement of coarse aggregate in concrete. Int J Adv Res Trend Eng Techn 2(7):1–6

16. Petrucciani A, Zaccara A, Matino I, Colla V, Ferrer M (2022) Flowsheet Model and simulation of produced slag in electric steelmaking to improve resource management and circular production. Chem Eng Trans 96:121–126
17. Biskri Y, Achoura D, Chelghoum N, Mouret M (2017) Mechanical and durability characteristics of high performance concrete containing steel slag and crystalized slag as aggregates. Constr Build Mater 150:167–178
18. Pasetto M, Baliello A, Giacomello G, Pasquini E (2017) Sustainable solutions for road pavements: a multi-scale characterization of warm mix asphalts containing steel slags. J CLEAN PROD 166:835–843
19. Kumar H, Varma S (2021) A review on utilization of steel slag in hot mix asphalt. Int J Pavement Res Tech 14:232–242
20. Liu J, Li C, Lin C, Han L, Ning T, Wu J, Lu A (2020) Use of steel slag and quartz sand-tailing for the preparation of an eco-friendly permeable brick. Inter J Appl Ceramic Technol 17(1):94–104
21. Dong Q, Wang G, Chen X, Tan J, Gu X (2021) Recycling of steel slag aggregate in Portland cement concrete: an overview. J Clean Prod 282:124447
22. Guo Y, Xie J, Zheng W, Li J (2018) Effects of steel slag as fine aggregate on static and impact behaviours of concrete. Constr Build Mater 192:194–201
23. Ríos JD, Vahí A, Leiva C, Martínez-De la Concha A, Cifuentes H (2019) Analysis of the utilization of air-cooled blast furnace slag as industrial waste aggregates in self-compacting concrete. Sustainability 11(6):1702
24. Guo Y, Xie J, Zhao J, Zuo K (2019) Utilization of unprocessed steel slag as fine aggregate in normal-and high-strength concrete. Constr Build Mater 204:41–49
25. Cahyani RAT, Rusdianto Y, (2020). *Concrete Performance with Ground Granulated Blast Furnace Slag as Supplementary Cementitious Materials.* Paper presented at the IOP Conference Series: Materials Science and Engineering.
26. Sanjeev N, Harish Kumar K, Kaza P (2019) Strength and durability characteristics of steel fibre reinforced concrete with mineral admixtures. Int J Eng Adv Technol 9:3893–3897
27. Parron-Rubio ME, Perez-Garcia F, Gonzalez-Herrera A, Oliveira MJ, Rubio-Cintas MD (2019) Slag substitution as a cementing material in concrete: mechanical, physical and environmental properties. Materials 12(18):2845
28. Parron-Rubio ME, Perez-García F, Gonzalez-Herrera A, Rubio-Cintas MD (2018) Concrete properties comparison when substituting a 25% cement with slag from different provenances. Materials 11(6):1029
29. Perez-Garcia F, Rubio-Cintas MD, Parron-Rubio ME, Garcia-Manrique JM (2020) Advances in the analysis of properties behaviour of cement-based grouts with high substitution of cement with blast furnace slags. Materials (Basel) 13(3):561. https://doi.org/10.3390/ma13030561
30. Surovtsov, M., Novoselova, Y., Slobozhankina, L., (2018). *On use of blast-furnace granulated ground slag in construction.* Paper presented at the IOP Conference Series: Materials Science and Engineering.
31. Yüksel, I., Siddique, R., Özkan, Ö., & Khatib, J. (2008). Effect of GGBFS and GSS on the properties of mortar. Excellence in concrete construction through innovation, 445–451.
32. Bendary, H. I., Heikal, M., & A Ali, M. (2023). Performance of imported granulated blast-furnace slag (IGBFS) rich cement against fire resistance. Egypt J Chem.
33. Lv X, Yang L, Li J, Wang F (2022) Roles of fly ash, granulated blast-furnace slag, and silica fume in long-term resistance to external sulfate attacks at atmospheric temperature. Cement Concr Compos 133:104696
34. Zhang S-L, Qi X-Q, Guo S-Y, Ren J, Chen J-Z, Chi B, Wang X-C (2021) Effect of a novel hybrid TiO2-graphene composite on enhancing mechanical and durability characteristics of alkali-activated slag mortar. Constr Build Mater 275:122154
35. Palod R, Deo S, Ramtekkar G (2019) Utilization of waste from steel and iron industry as replacement of cement in mortars. J Mater Cycles Waste Manage 21:1361–1375
36. ASTM, A. (2011). Standard test methods for fineness of hydraulic cement by air-permeability apparatus. ASTM International.
37. ASTM. (2008). ASTM C191–08: Standard test method for normal consistency and setting time of hydraulic cement. In: ASTM International West Conshohocken, PA, USA.
38. Aziz MAE, Aleem SAE, Heikal M, Didamony HE (2005) Hydration and durability of sulphate-resisting and slag cement blends in Caron's Lake water. Cem Concr Res 35(8):1592–1600
39. Abd El-Aleem S, Abd-El-Aziz M, Heikal M, El Didamony H (2005) Effect of cement kiln dust substitution on chemical and physical properties and compressive strength of Portland and slag cements. Arab J Sci Eng 30(2B):264
40. El-Alfi E, Radwan A, Abed El-Aleem S (2004) Effect of limestone fillers and silica fume pozzolana on the characteristics of sulfate resistant cement pastes. Ceramics Silikaty 48(1):29–33
41. Mohamed SAE-A, Ragab AE-R (2014) Physico-mechanical properties and microstructure of blended cement incorporating nano-silica. Int J Eng Res Tech 3(7):339–358
42. Sufee, H. (2007). Comprehensive studies of different blended cements and steel corrosion performance in presence of admixture. Ph. D. Thesis, Faculty of Science, Fayoum University, Fayoum, Egypt,
43. Standard, A. (2007). C150–07. Standard Specification for Portland Cement.
44. Heikal M (2006) Effect of temperature on the structure and strength properties of cement pastes containing fly ash alone or in combination with limestone. Ceramics Silikaty 50(3):167
45. Valosov, V. (1988). The mechanism of increase of concrete strength at introduction of micro-fillers. Concr. Res. (USSR), 9–11.
46. Heikal M (2004) Effect of calcium formate as an accelerator on the physicochemical and mechanical properties of pozzolanic cement pastes. Cem Concr Res 34(6):1051–1056
47. Eckart A, Ludwig H, Stark J (1995) Hydration of the 4 main Portland-cement clinker phases. Zement-Kalk-Gips 48(8):443–452
48. Heikal M, Helmy IM, Awad S, Ibrahim NS (2020) Performance of silica-nano-particles on the physicochemical, and microscopic characteristics of blended and composite cement. Ceramics-Silikáty 64(3):320–337
49. Gu C, Yao J, Yang Y, Huang J, Ma L, Ni T, Liu J (2021) The Relationship of compressive strength and chemically bound water content of High-volume fly ash-cement mortar. Materials (Basel) 14(21):6273. https://doi.org/10.3390/ma14216273
50. Tang S, Cai X, He Z, Shao H, Li Z, Chen E (2016) Hydration process of fly ash blended cement pastes by impedance measurement. Constr Build Mater 113:939–950
51. Reiterman P, Holčapek O, Davidová V, Jaskulski R, Keppert M (2019) Estimation of hydration degree of blended cements with the help of k-values. Materials 12(15):2420
52. Scrivener KL, Juilland P, Monteiro PJ (2015) Advances in understanding hydration of Portland cement. Cem Concr Res 78:38–56
53. Bakharev T (2005) Durability of geopolymer materials in sodium and magnesium sulfate solutions. Cem Concr Res 35(6):1233–1246
54. Alonso C, Fernandez L (2004) Dehydration and rehydration processes of cement paste exposed to high temperature environments. J Mater Sci 39(9):3015–3024

55. Bensted, J. (1994). Applications of Infrared Spectroscopy to cement hydration. Paper presented at the Society of chemical industry construction materials group and institute of materials meeting on techniques for characterization of cement hydration, society of chemical industry.
56. Mohamed SAE-A, El S (2015) Activation of granulated blast-furnace slag using lime rich sludge in presence and absence of rice husk ash. Inter J Innovat Tech Exploring Eng 5(3):43–51
57. Delgado AH, Paroli RM, Beaudoin JJ (1996) Comparison of IR techniques for the characterization of construction cement minerals and hydrated products. Appl Spectrosc 50(8):970–976
58. Davidovits, J. (1976). Solid phase synthesis of mineral block-polymer by low temperature polycondensation of alumino-silicate polymers.
59. Yip CK, Lukey GC, Provis JL, Van Deventer JS (2008) Effect of calcium silicate sources on geopolymerisation. Cem Concr Res 38(4):554–564
60. Mostafa N, El-Hemaly S, Al-Wakeel E, El-Korashy S, Brown P (2001) Characterization and evaluation of the hydraulic activity of water-cooled slag and air-cooled slag. Cem Concr Res 31(6):899–904
61. Ramachandran, V. S. (1969). *Applications of differential thermal analysis in cement chemistry*: Chemical Publishing Company.
62. Morsy MS, Galal A, Abo-El-Enein S (1998) Effect of temperature on phase composition and microstructure of artificial pozzolana-cement pastes containing burnt kaolinite clay. Cem Concr Res 28(8):1157–1163
63. Yazıcı Ş, Sezer Gİ, Şengül H (2012) The effect of high temperature on the compressive strength of mortars. Constr Build Mater 35:97–100
64. Tantawy, M. (2008). The Physico-chemical properties of pozzolanic-filled cement pastes. Ph. D. Thesis, El-Menia University, Egypt,
65. Heikal M, Aiad I (2008) Influence of delaying addition time of superplasticizers on chemical process and properties of cement pastes. Ceramics Silikaty 52(1):8
66. El-Didamony H, Abd El-Rahman E, Osman RM (2012) Fire resistance of fired clay bricks–fly ash composite cement pastes. Ceram Int 38(1):201–209
67. Ševčík V, ŠkváRa F, ŠkváRa F (2001) High-temperature properties of a binder based on gypsum-free Portland cement over the temperature range of 20 to 1200° C. Ceramics-Silikty 45(4):151–157
68. Esteves LP (2011) On the hydration of water-entrained cement–silica systems: combined SEM, XRD and thermal analysis in cement pastes. Thermochim Acta 518(1–2):27–35
69. El-Didamony H, Amer AA, El-Hoseny S (2016) Recycling of low-grade aluminosilicate refractory brick waste product in blended cement. J Therm Anal Calorim 125:23–33
70. Ramachandran VS, Paroli RM, Beaudoin JJ (2002) Delgado AH. Handbook of thermal analysis of construction materials, William Andrew